Journal of Environmental Management 316 (2022) 115212

Contents lists available at ScienceDirect

Journal of Environmental Management

journal homepage: www.elsevier.com/locate/jenvman

Post-fire management effects on hillslope-stream sediment connectivity in a Mediterranean forest ecosystem

J. González-Romero [a,*], M. López-Vicente [b], E. Gómez-Sánchez [a], E. Peña-Molina [a], P. Galletero [a], P. Plaza-Álvarez [a], A. Fajardo-Cantos [a], D. Moya [a], J. De las Heras [a], M.E. Lucas-Borja [a]

[a] University of Castilla-La Mancha (UCLM), Technical School of Agricultural and Mountain Engineering (ETSIAM), Albacete, 02071, Spain
[b] AQUATERRA Research Group, Advanced Scientific Research Centre (CICA), Universidade da Coruña, Coruña, 15071, Spain

ARTICLE INFO

Keywords:
Forest fire
Post-fire management
Sediment connectivity
Hillslope erosion
Wildfires

ABSTRACT

Forest fires intensify sediment transport and aggravate local and off-site consequences of soil erosion. This study evaluates the influence of post-fire measures on structural and functional sediment connectivity (SC) in five fire-affected Mediterranean catchments, which include 929 sub-catchments, by using the "aggregated index of connectivity" (AIC) at two temporal scenarios: I) immediately after the fire and before implementing post-fire practices ('Pre-man'), and II) two years after the fire ('Post-man'). The latter includes all the emergency stabilization practices, that are hillslope barriers, check-dams and afforestation. The stream system was set as the target of the computation (STR), to be representative of intense rainfall-runoff events with effective sediment delivery outside the catchments. Output normalization (AIC_N) allows comparing the results of the five basins between them. The sedimentological analysis is based on specific sediment yield (SSY) –measured at the check-dams installed after the fire –, and this data is used for output evaluation. Stream density and slope variables were the most influential factors on $AIC_{N\text{-}STR}$ results at the sub-catchment scale. Post-fire hillslope treatments (barriers when built in high densities and afforestation) significantly reduced $AIC_{N\text{-}STR}$ in comparison with untreated areas in both structural and functional approaches. Despite the presence of hillslope treatments, the higher erosive rainfall conditions resulted in higher $AIC_{N\text{-}STR}$ values in the Post-man scenario (functional approach). A positive and good correlation was found between the measured SSY and the $AIC_{N\text{-}STR}$ changes due to the post-fire practices and vegetation recovery, showing the good correspondence of the computation results and the real sediment dynamics of the studied catchments. Overall, AIC_N demonstrated to be a useful and versatile tool for post-fire management, which needs further research to optimize its applicability.

1. Introduction

Forest fires are common natural phenomena in Mediterranean fire-prone ecosystems (Fernández-García, 2019). At short- and medium-term, forest fires modify the natural dynamic –magnitude and patterns– of runoff generation, favoring higher rates of soil erosion, and sediment transport and yield (Rodrigo-Comino et al., 2020). During this period, erosion processes are enhanced, and the action of heavy rainfall events may produce major and irreversible disturbances. In fact, in the Mediterranean basin, where rainfall events are irregularly distributed during the year, the risk of high erosion rates due to extreme rainfall events is particularly high after wildfires (Panagos et al., 2015). These changes affect the different catchment parts (e.g. headwaters, hillslopes, lowlands, arable soils, areas with natural vegetation, ravines, ephemeral and permanent streams) due to the loss of the plant cover and the heat-induced changes in soil properties. All in all, the enhanced flow can increase hillslope erosion and sediment delivery (Moody et al., 2005) and can also mobilize fine ash particles and transport them downstream in suspension, especially during the first events after forest fire, affecting reservoir water quality and human health (Robichaud et al., 2008; 2010).

In this context, post-fire management strategies aim to reduce the magnitude of the impact generated by forest fires and extreme rainfall events in the short term (Vieira et al., 2016), and can be crucial to the ecosystem recovery in the long term. The principal objective of these measures is to decrease runoff generation and velocity, and linked processes like sediment transport and yield, water quality affection or floods that can cause material and human losses (Robichaud et al.,

* Corresponding author.
E-mail address: javier.gromero@uclm.es (J. González-Romero).

https://doi.org/10.1016/j.jenvman.2022.115212
Received 27 October 2021; Received in revised form 25 April 2022; Accepted 30 April 2022
Available online 10 May 2022

2013). Among emergency stabilization techniques, we can find two types of measures, those which seek to achieve a protective cover of soil such as mulching or seedling, or those which aim to the retention of runoff and sediment by building physical barriers on hillslopes and streams (Girona-García et al., 2021) as log erosion barriers, contour felled log debris, or check dams (Aristeidis and Vasiliki, 2015; Badía et al., 2015). These emergency measures are commonly built-in high severity areas during the first post-fire years or window of disturbance (Prats et al., 2016). If the vegetation natural regeneration does not ensure the ecosystem restoration, afforestation is a common post-fire strategy to achieve the desired soil cover and thus reduce soil losses (Cerdà et al., 2017). Nevertheless, the effectiveness of post-fire management strategies will always rely on their design, location and external forces as fire severity or post-fire climatic conditions (Badía et al., 2014). Hillslope log- and debris-barriers efficiency has been questioned by authors like RobichaudRobichaud (2000) or Aristeidis and Vasiliki (2015), who observed nule or low efficiency of these barriers retaining sediment, especially in steep slopes. These bioengineering structures involve complex and hazardous manual operations, and the existence of field materials in the area, which usually implies high labor (Albert-Belda et al., 2019). Also the masonry gabion and concrete check-dams, which have been traditionally installed in ephemeral channels in Spain after forest fires or as hydrological control works (Boix-Fayos et al., 2020) are under debate, due to their high economic cost, requiring the use of heavy machinery or for being considered short-term solutions (Quiñonero-Rubio et al., 2016). Afforestation projects, which are usually successful, in some cases may lead into enhanced erosion processes, as species as pines can increase soils' water repellency (Cerdà et al., 2017). The debate about post-fire measures benefits and shortcomings is open, which hinders the development of proper restoration strategies (Albert-Belda et al., 2019; Rulli et al., 2013). Understanding the interactions of the different measures will definitely help to establish criteria for decision making (Boix-Fayos et al., 2020). The use of efficient tools to properly plan and evaluate the effects of these strategies sets a path for optimizing economic and human resources. In the last years, terms like sediment or hydrological connectivity have emerged as crucial concepts in watershed and land management and its application to explain different processes has been widely spread, including fire-affected areas (e.g. Martínez-Murillo and López-Vicente, 2018; Lopez-Vicente et al., 2020; Martini et al., 2020).

Sediment connectivity (SC) can be defined as the level of predisposition of a catchment to water and sediment transport within it, via linking connections between its components (Heckmann et al., 2018). Through initiatives like the European Research 'Connecteur' COST action ES1306, the SC concept has been studied and applied in many cases and different locations during the last years (Keesstra et al., 2020). Two types of SC can be identified, namely structural SC and functional SC, the first one is related with physical linkages between landscape components and the second one is more based on natural processes. Structural SC can be defined as a system's potential to allow sediment transport within it, depending on the spatial configuration and linkages of its components (Heckmann and Vericat, 2018). In contrast, functional SC can be defined as the transfer of sediment in a catchment derived from different geomorphic and hydrological processes (Cavalli et al., 2019, Masselink et al., 2016). Based on these descriptions, we can assume that structural SC will be more related with the catchment's topography or vegetation distribution, while functional SC will depend on sediment deposition and detachment usually produced as a consequence of hydrological processes. Structural and Functional SC are interrelated, as changes on structural components of a catchment (vegetation removal after wildfire affection), can lead into enhanced runoff and erosion processes. On the other hand, these enhanced erosion processes can lead into structural changes as the appearance of rills and gullies at the hillslopes. Sediment connectivity can also be studied under different spatial scales (Heckmann et al., 2018). The first one is the hillslope scale or lateral connectivity, which is related with the processes of sediment transport from the hillslopes to the stream network. We can also study SC at the channel network scale (longitudinal connectivity), assessing the connection between the different channels of the catchment and how it affects to sediment transport. Finally, we can study SC at the catchment scale, which comes from the interaction of the previous two, considering the sediment transport from the hillslopes to the outlet through the stream network.

Among the different approaches to quantify SC, the development of SC indices has been one of the more recurrent research lines. Most of the available indices reflect the degree of structural SC of a system/catchment, existing still limitations to quantify functional SC. One of the most used indices is the "index of sediment connectivity" (IC) developed by Borselli et al. (2008). This index calculates a dimensionless value for each pixel, based on the effect of the land use and topographic characteristics of the upslope drainage area and the downslope flow path. The IC index has been tested under several environments and conditions (Estrany et al., 2019; López-Vicente, 2017; Ortíz-Rodriguez et al., 2019), and its capacity to map SC has been widely proven. Nevertheless, as said above, the main weak spot of the IC index and modifications as the one performed by Cavalli et al. (2013), is the to reflect dynamic processes (functional SC). In the last years, researchers have tried to overcome this by modifying the existing indices (López-Vicente and Ben-Salem, 2019) or working at different temporal scales (Burguet et al., 2017, Lopez--Vicente et al., 2021). Authors like Heckmann et al. (2018) have identified that, despite the great potential of SC approaches to land hydrological management, their integration into decision-making protocols is still lacking. Regarding the assessment of forest fires' effects and post-fire management strategies on a catchment hydrological response and erosion dynamics, SC indices can provide a simple numerical approach which requires less inputs than modelling (Lopez-Vicente et al., 2021). The disconnectivity of a system, involve that its components and/or processes do not influence each other because they are too remote in space or time, or that certain thresholds must be exceeded to allow connectivity (Wohl et al., 2019). Overall, post-fire management strategies aim to modify those thresholds and produce certain disconnectivity in the hydrological system of the catchment, reducing runoff generation (Robichaud et al., 2013), laminating overland flow and reducing sediment delivery from the hillslopes to the channels (Shakesby, 2011). In Spain, Martínez-Murillo and Lopez-Vicente (2018) applied the previously appointed IC index to evaluate the effects of fire affection and different post-fire measures, such as salvage logging or check-dam construction, in SC in headwater sub-catchments. More recently López-Vicente et al. (2020) evaluated the capability of different SC indices to reflect fire-induced changes and post-fire management measures effects on SC in the SE of Spain. The study concluded that the "aggregated index of sediment connectivity" (AIC), developed by López-Vicente and Ben-Salem (2019), reflected these changes in a better way due to the addition of variables as rainfall erosivity, which allowed to assess functional SC changes. Also in Spain, other studies evaluated the effectiveness of different hillslope barriers to reduce structural SC at a small basin scale (Lopez-Vicente et al., 2021), or the effect of straw mulch application on SC (Fernández et al., 2020). In other regions, Martini et al. (2020) studied the interactions between SC (IC index) and fire severity in central Chile, while Ortíz-Rodríguez et al. (2019) studied the changes in SC and hydrological efficiency after forest fire in Sierra Madre (Mexico) by using the IC and introduced the lateral hydrological efficiency index (LHEI).

In spite of the recent investigations, there are few studies assessing SC after fire and the effect of the installation and location of post-fire emergency stabilization measures on it, highlighting the necessity to open new investigation lines regarding this topic. Additionally, it remains as a crucial issue to assess SC derived from extreme rainfall events that produce an effective sediment yield throughout the channels, and how post-fire practices affect this process. Therefore, the main objective of this study is to assess the suitability of the aggregate index of sediment connectivity (AIC) to evaluate the effects of post-fire emergency

stabilization measures in Mediterranean catchments. More specifically:

- At the sub-catchment and hillslope scale
- Considering that an effective sediment transport through the stream network takes places in the catchments
- Under static (structural connectivity) or dynamic (functional connectivity) rainfall conditions

To accomplish that, we simulate structural and functional SC in five burned catchments in the SE of Spain where different post-fire management measures were carried out. The computation was realized using the aggregated index of connectivity (AIC) in two different scenarios (pre- and post-management), and establishing the stream network as target of the computations. The results are evaluated with the measured area specific sediment yield (SSY) in the check-dams which were installed after the fire. We hypothesize that structural and functional connectivity are significantly reduced by post-fire management strategies at the hillslope scales, and that the AIC index reflects the disconnectivity produced by post-fire emergency measures.

2. Material and methods

2.1. Study area and wildfire characteristics

This study was conducted in five catchments located in SE of Spain, more precisely, in 'Sierra de los Donceles' at the borderline between the provinces of Albacete and Murcia (Fig. 1). This area was affected by a forest fire in July 2012, being an intense and short event, which burned around 6500 ha between the two provinces. Fire severity was mostly considered as moderate-high based on the results of Gómez-Sánchez et al. (2017). The five considered catchments are named Postes (1090 ha), Conejo (388 ha), Grillo (198 ha), Piñero (495 ha) and Rayares (Rayares1081 ha) (Fig. 1), and their elevation and mean slope gradient ranges from 304 to 808 m a.s.l and 28.9%–39.5% respectively. Regarding catchments morphometry, as it can be observed in Table 1, the catchment with the highest elongation ratio, and, by hence the most circular shaped one was Piñero. This catchment was also the one with a higher stream density with 84 m ha^{-1}. On the other hand, Grillo was the most elongated catchment and also the one with the lowest stream density (69 m ha^{-1}).

Although no permanent stream exists in the study area, ephemeral streams have sculpted the landscape, creating clear scars that act as effective sediment-delivery channels, since the headwater areas, crossing the middle part of the catchments and reaching the outlets. Channel morphology varies along the channels of the different catchments; in the upper areas, where Jurassic bedrocks as dolomitic limestones and conglomerates are predominant, channels are narrow and not very incised with vegetation completely colonizing the channel bed. At medium and lower parts, quaternary colluviums appear, channels present incised thalwegs with a width of 10–25 m and a deep of around 5 m depending on the area, streambanks are steep, and vegetation proliferates at them. Close to the outlet, the channels of the catchments Piñero and Rayares, which disgorge into Segura River (Fig. 1), turn to steep ravines while in the other three catchments if less incised the channel has eroded to bedrock in some parts. These channels are mainly narrow (10–20 m), the flow is ephemeral (associated with storms and rainy periods), and the streambanks are commonly steep. The main characteristics of the stream systems can be observed in Table 1.

The climate is semi-arid Mediterranean, and the area is located on the meso-Mediterranean bioclimatic belt (Rivas-Martínez et al., 2002). The average annual rainfall is ca. 320 mm, and the mean annual temperature was 16.2 °C for the period 1990–2014 (AEMET – Spanish Agency of Meteorology). The highest rainfall amount is usually recorded during fall and spring, and summers are very dry. As it is common in Mediterranean environments, rainfall distribution is very irregular, long dry periods are alternated with short high intensity events. For the periods included in the present study, several examples of this phenomenon are observed. In the 2012–2013 period, with a total annual rainfall of 444 mm, we found that 98 mm were recorded on 28/sept/2012 with a maximum intensity for 30 min (I_{30}) of 17.62 mm h^{-1}. The more intense events took place during that period, on 12/oct/2012 with I_{30} of 44.8 mm h^{-1} were recorded for a 23 mm rainfall event. For the 2014–2015 period, events like the one recorded on 24/Mar/2015 with 66.8 mm and I_{30} = 80 mm h^{-1} also confirm this theory.

With regard to vegetation, previous to forest fire, most of the catchments' surface was covered by a *Pinus halepensis* open forest, escorted by rich layers of companion shrubs and herbs. This conifer forest appeared mostly in north-facing hillslopes while in the south-

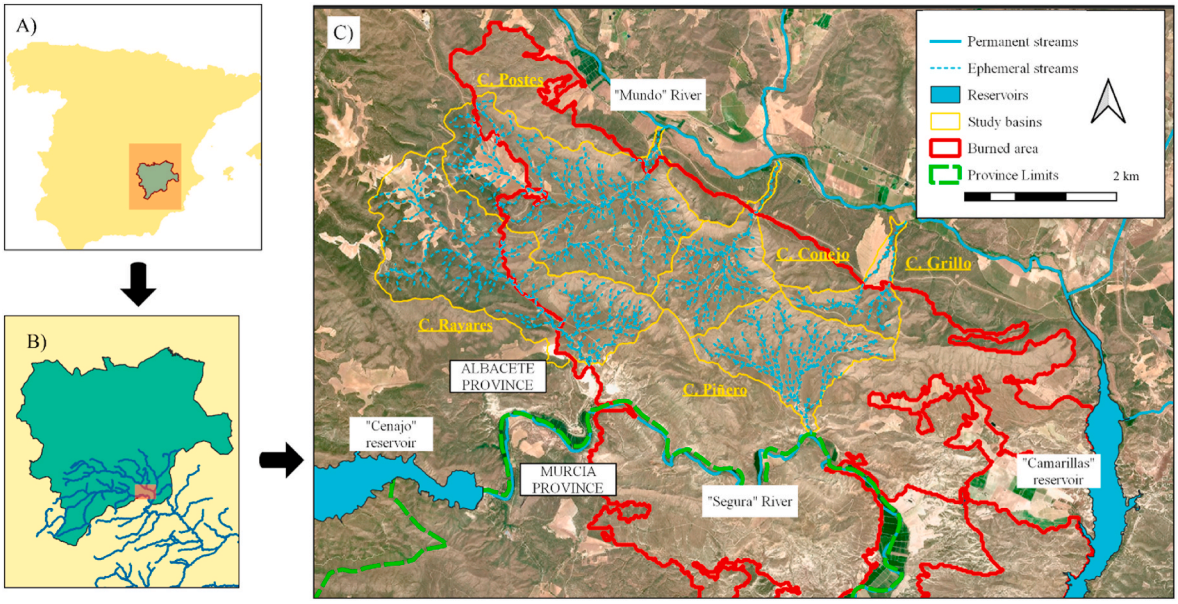

Fig. 1. A) In blue the location of Albacete province within Spain. B) Location of the study area in the SE of albacete and within the Segura river basin. C) Location of the wildfire and the selected study catchments in the 'Sierra de los Donceles'. (For interpretation of the references to colour in this figure legend, the reader is referred to the Web version of this article.)

Table 1
Main physiographic characteristics of the five catchments. Catchment morphometry (elongation ratio value): elongated (<0.7), less elongated (0.7–0.8), oval (0.8–0.9), and circular (>0.9) (Chandrashekar et al., 2015).

Catchment	Drainage area	Elongation Ratio	Slope Gradient	Predominant aspect	Stream density	Main stream length	Tributary segments	Total length stream system
(ID)	(ha)	–	(%)	(Class)	($m \cdot ha^{-1}$)	(km)	(nº)	(km)
Postes	1090	0.637	28.9	North-West	78	9.395	171	8.517
Conejo	388	0.638	38.5	North-West	78	6.279	70	3.04
Grillo	198	0.525	39.6	North-West	69	5.255	36	1.392
Piñero	495	0.802	37.6	South	84	4.474	86	4.155
Rayares	1081	0.622	34.1	South-West	70	10.126	152	7.456

facing ones, dwarf scrubs as *Salvia rosmarinus* or *Thymus vulgaris* and a dense herbal layer of *Macrochloa tenacissima* and *Brachypodium retusum* were predominant. The years following the fire, these shrub and herbal layers have regenerated homogeneously, and pine regeneration can be observed in the slopes where the open forest was present.

2.2. Evaluated temporal scenarios

Two annual scenarios were established to study those periods which were of interest and to fulfil the objectives of the study:

I) The "Pre-man" scenario (01/jul/2012–30/jun/2013). Representative of the period before post-fire management actions, which also corresponds with the situation immediately after the wildfire.
II) The "Post-Man" scenario (01/jul/2014–30/jun/2015). Representative of the period which followed post-fire management actions. To simulate this scenario the post-fire measures were considered when preparing index inputs.

Both scenarios represent a one-year period and can be considered comparable concerning vegetation phenology and hydrologic year duration. The hydrological year 2013–2014 was not considered as it was not fully representative of any of the scenarios.

2.3. Post-fire management measures

After the July 2012 wildfire, numerous measures were planned and implemented. The restoration works were finished during the next year after the fire (2013) as it is showed in Fig. 2. Two main types of measures can be categorized: hillslope measures (hillslope barriers and afforestation) and channel measures (check-dams). Hillslope measures were carried out in hillslopes of <50% of slope gradient and mainly north-faced where the availability of woody material allowed to build them. In the south-faced slopes, barriers were built in lower densities, but

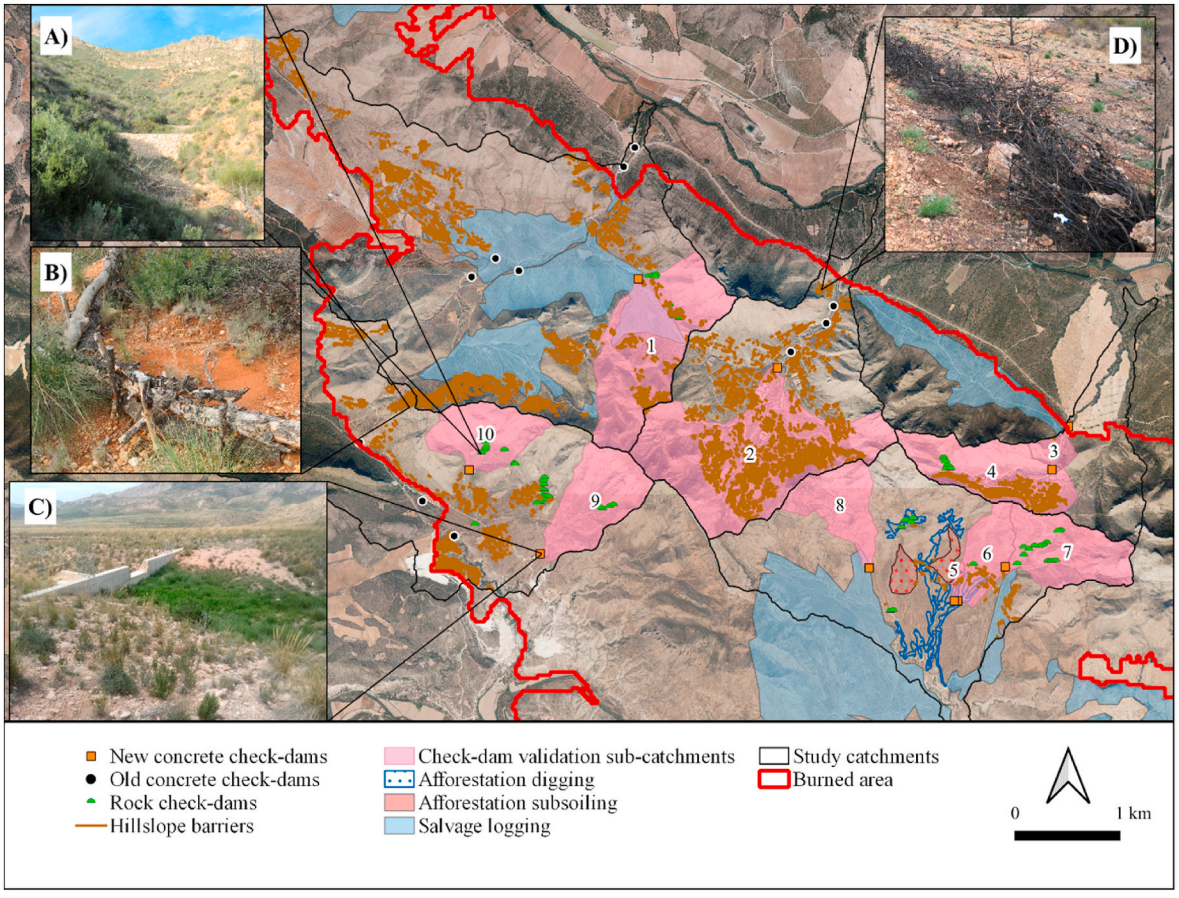

Fig. 2. Location of the main channel and hillslope measures carried out at the post-fire management. In picture the main post-fire measures: (A) Rock check-dam (B) Log erosion barriers, (C) Concrete check-dam, and (D) Contour felled log debris.

afforestation was also performed. The main undertaken hillslope treatments were:

I) Hillslope barriers (HB):
   i. Log erosion barriers ((A) in Fig. 2): The maximum length of the barriers is 15 m and by average there were a 10 m distance between them; they formed swaths which followed the contour lines and using a staggered pattern. The structures had a maximum height of 25 cm or 40 cm (if located immediately upstream of a trail or a road) and were fixed to the ground using stakes or using the remaining stumps. Residual branches were piled upstream the logs to be used as an energy dissipater.
   ii. Contour felled log debris ((B) in Fig. 2): Branches and log debris were stacked and fixed with stakes to the ground following the contour lines.

II) Afforestation ((C) in Fig. 2): Afforestation was executed exclusively in Piñero catchment (mainly a south-faced catchment) during the spring of 2013 and shrub species were used on it with a density of 500 plants·ha^{-1} for all the species. Among those species *Arbutus unedo*, *Rhamnus lycioides*, *Nerium oleander*, *Salvia rosmarinus*, *Olea europaea* var *sylvestris*, *Phyllirea angustifolia* or *Viburnum tinus* were used. Before afforestation, two different soil preparation methods took place, one area's soil was prepared using mechanical subsoiling (14.82 ha). At the rest of the treated area (21.58 ha), soil preparation involved mechanical digging, using an excavator and opening holes of 40 × 40 cm or 60 × 60 cm and a depth of 30, 40, and 60 cm.

III) Salvage logging: Local crews felled the trees using a chainsaw and a small crawler skidder transported and piled the logs. Skid trails were opened throughout the logged hillslopes during the works.

With regard to the measures performed in the channels after the wildfire, we mainly observe:

I) Concrete check-dams: 10 of these structures were built in throughout the studied catchments at the main channels to retain sediment loads and protect downslope facilities. The concrete check-dams height ranged between 3 and 6.5 m having widths of 21–39 m. Due to the magnitude of the works, the structures were in accessible areas close to the main trails or unpaved roads. 12 concrete check-dams were already built in the area before 2012 (Fig. 2), these check-dams were also of a significant size (15–20 m of width and 4–5 m of height).

II) Rock check-dams: In secondary channels and mainly in the upper areas of the south-faced catchments, a total of 66 rock check-dams were built. The maximum height of these structures is 2 m depending on the channel's slope. In many cases several rock check-dams were built in the same channel, depending the distance between them on the height of the downstream one and the channel slope with a minimum of 2 m of distance.

The density of the different post-fire measures for each catchment are showed in Table 2.

Table 2
Post-fire management measures density for each catchment, hillslope barriers, afforestation, small rock check-dams rock check-dams and concrete check-dams.

Catchment	Hillslope barriers density	Afforestation area	Rock check-dams	Concrete check-dams
(ID)	(m·ha^{-1})	(ha)	(number)	(number)
Postes	36.96	–	8	6
Conejo	86.71	–	–	4
Grillo	27.05	–	7	2
Piñero	3.54	35.62	23	4
Rayares	17.56	–	30	4

2.4. Sediment connectivity index

The selected sediment connectivity index for this study, was the Aggregated Index of runoff and sediment Connectivity (AIC). López-Vicente et al. (2020) studied how four indices of SC performed to measure hillslope-channel and hillslope-outlet SC in three different subcatchments located in the southeast of Spain. They observed that the most suitable index was this aggregated index (AIC; López-Vicente and Ben-Salem, 2019), which is a modified and extended version of the equation developed by Borselli et al. (2008), and later modified by Cavalli et al. (2013).

This index is made up of two components, the upslope component (D_{up}), which considers the potential descending routing of the runoff and sediment produced upslope. The downslope component (D_{dn}), which signifies the probability of sediment and runoff of reaching a specified sink along the flow path. AIC is calculated following equations (1) and (2):

$$AIC_k = \log_{10}\left(\frac{D_{up,k}}{D_{dn,k}}\right) = \log_{10}\left(\frac{\overline{R_t}\cdot\overline{RT}\cdot\overline{C_t}\cdot\overline{K_P}\cdot\overline{S}\cdot\sqrt{A_k}}{\sum_{k=i}^{n}\frac{d_i}{\overline{AWC_i}}}\right) \quad (1)$$

$$AWC_i = R_{ti}\cdot RT_i\cdot C_{ti}\cdot K_{Pi}\cdot S_i \quad (2)$$

where $\boldsymbol{d_i}$ is the flow path length downstream, $\boldsymbol{AWC}$ is the aggregated weighting factor, $\boldsymbol{R_t}$ is the normalized rainfall erosivity factor for the period $\boldsymbol{t}$, $\boldsymbol{RT}$ is the roughness of the terrain factor that represent how the small changes on slope gradient can influence overland flow velocity (Grohmann et al., 2011), $\boldsymbol{C_t}$ is the RUSLE vegetation management factor for the period $\boldsymbol{t}$, $\boldsymbol{K_P}$ is the soil permeability factor and $\boldsymbol{S}$ is the slope gradient factor (m · m^{-1}). The values of each factor were normalized and ranged between 0.001 and 1.

To calculate the $\boldsymbol{R_t}$ factor, we calculated rainfall erosivity ($\boldsymbol{EI_{30t}}$) at monthly scale as the sum of the erosivity of the different rainfall events following the next equations:

$$EI_{30} = (E)(I_{30}) = \left(\sum_{K=1}^{m} e_r \Delta V_r\right) I_{30} \quad (3)$$

$$e_r = 0.29[1 - 0.72\exp(-0.082 i_r)] \quad (4)$$

$$i_r = \frac{\Delta V_r}{\Delta t_r} \quad (5)$$

where $\boldsymbol{m}$ (n) is the number of temporal intervals established for each rainfall event; $\boldsymbol{e_r}$ (MJ · ha^{-1}·mm^{-1}) is the kinetic energy of a rainfall event for the $\boldsymbol{r}$ period; $\boldsymbol{\Delta V_r}$ (mm) is the volume of rainfall during the $\boldsymbol{r}$ period; $\boldsymbol{I_{30}}$ (mm · h^{-1}) is the maximum rainfall intensity occurred in 30 min for each rainfall event, $\boldsymbol{I_r}$ (mm · h^{-1}) is the rainfall intensity for the $\boldsymbol{r}$ period; and $\boldsymbol{\Delta t_r}$ (min) is the $\boldsymbol{r}$ period duration.

If the resulting $\boldsymbol{EI_{30t}}$ values in equation (3) were lower than 0.01, they were converted to $\boldsymbol{EI_{30t}} = 0.01$, in order to prevent computational errors. In this study, the duration of the $\boldsymbol{t}$ period (equations (1) and (2)) was always of one average year.

Although the $\boldsymbol{R_t}$ factor is a key addition of AIC which allows to better study functional SC (real sediment transport dynamics), in our case of study, due to the great rainfall-erosivity differences between scenarios (Table 3a), we considered the importance of determining structural SC. Calculating structural SC maps allowed us to assess the effect of post-fire management under similar rainfall conditions.

Therefore, in addition to the AIC functional (AIC_F) approach, for the same scenarios (Pre-man and Post-man) and target (stream), structural SC maps (AIC_S) were calculated. In this approach, the $\boldsymbol{R_t}$ factor a value equal to 1. As the Post-man scenario had the highest rainfall erosivity,

Table 3a
Changes of the rainfall erosivity factor (R_T) values of the studied scenarios. EI30: Calculated value of rainfall erosivity; Rt: Rainfall erosivity factor in the AIC.

Scenario	Dates (duration)	Rainfall (mm · year^{-1})	EI_{30} (MJ mm · ha^{-1}·h^{-1}·yr^{-1})	R_t (0–1)
Pre-man	Jul2012-Jun2013	440	619.2	0.540845
Post-man	Jul2014-Jun2015	410	1145.0	1.000000

the $\boldsymbol{R_t}$ factor was equal to 1 in both the AIC_F and AIC_S maps. Thus, three SC maps were obtained, two for the Pre-man scenario and one for the Post-man scenario.

2.5. Computation inputs and target

A 2 × 2 m digital elevation model (DEM) was generated for each temporal scenario. To do so, we used two LiDAR point clouds provided by the Spanish Nacional Centre of Geographic Information (IGN). The clouds were dated 2009 (Pre-man scenario) and 2016 (Post-man scenario). The clouds were processed with LAStools and ArcGIS© 10.5 software. The local depressions of the resulted DEMs were removed using the Planchon and Darboux algorithm (available in SAGA© *2.1.2*), ensuring the flow path lines continuity across the hillslopes and in the streams network. A minimum gradient of 0.01° was considered to allow the flow to cross the filled sinks. After pre-processing the DEMs, we calculated flow accumulation maps by running the Deterministic Infinity (D-Inf or D∞) algorithm available in SAGA© 2.1.2. This approach has several advantages over single-flow approaches (Cavalli et al., 2013) and represents in a more realistic way sediment paths. We use the resultant maps to define the boundaries of the different catchments.

Regarding the aggregated weight factor (AWC_i) inputs: To calculate the Slope gradient ($\boldsymbol{S_i}$) we used the ArcGIS© 10.5 slope tool and values (%) were expressed on a per unit bases. We set a minimal value of $\boldsymbol{S_i} = 0.005$ and a maximum value of $\boldsymbol{S_i} = 1$, adjusting the pixels with values below or above those. The roughness of the terrain ($\boldsymbol{RT_i}$) factor was calculated using the DEMs and the 'Residual Analysis (Grid)' tool of SAGA© 2.1.2. coming as a result of the normalized and inverse values of the standard deviation of the slope gradient. A minimum value of 0.001 of $\boldsymbol{RT_i}$ was set to avoid errors at the calculus.

The soil permeability ($\boldsymbol{K_P}$) factor (Table 3b) was calculated using the lithostratigraphic units map (1:50.000) of the Spanish Geological Institute (IGME). The "moderate" permeability areas took a $\boldsymbol{K_P}$ value of 1, while the "high" and "very high" permeability areas took $\boldsymbol{K_P}$ values of 0.667 and 0.333 respectively. $\boldsymbol{K_P}$ values didn't suffer changes between scenarios.

Regarding the $\boldsymbol{R_t}$ factor (Eq. (3)), it was calculated using the rainfall records every 5 min of the "Cenajo" reservoir weather station (Fig. 1), of the Segura River basin stations network (data source: CHSegura-SAIH; code 04A02P01). Therefore, there were no spatial changes on $\boldsymbol{EI_{30}}$, and a unique $\boldsymbol{R_t}$ value was applied for the whole study area at each temporal scenario.

Table 3b
Mean value of the AIC inputs for the two studied scenarios (pre- and post-management) and studied catchments. Vegetation management (C), soil permeability (Kp), and roughness of the terrain (RT) factors.

Catchment	Land use factor $\overline{C}$ (Pre-man)	Land use factor $\overline{C}$ (Post-man)	Soil permeability factor (Kp)	Roughness of the terrain factor (RT)
(ID)	(Mean)	(Mean)	(Mean)	(Mean)
Postes	0.11	0.095	0.28	0.94
Conejo	0.11	0.09	0.32	0.94
Grillo	0.11	0.098	0.24	0.94
Piñero	0.13	0.10	0.31	0.94
Rayares	0.07	0.065	0.29	0.94

The $\boldsymbol{C_t}$ factor input maps were calculated using the SIOSE land cover map (Source: Spanish Geographical Institute (IGN)). We used two different land cover maps, one corresponded with the year 2011 (pre-wildfire vegetation conditions) and the other with 2014 (two years after the wildfire) (Supplementary Figures 1, 2). Each polygon of these SIOSE maps is the combination of different covertures (Crops, conifer forest, shrubs, grassland …) and percentages are assigned to each one (e.g. 60% of conifer forest; 25% of dense shrubs; and 15% of herbs). Additions such as trails and the steep banks of the gullies with bare soil were made to complete the maps due to their relevance on soil erosion and flow pathways.

Once the land cover maps were completed for the two temporal scenarios, the C-factor values were assigned using the values proposed by Panagos et al. (2015) (Supplementary Table 1). Additionally, for the Pre-management scenario we multiplied the pre-fire C-factor map (2011) with a weighted burn severity map (Martínez-Murillo and López-Vicente, 2018) based on the values proposed by (Yochum and Norman, 2015): Low burn severity = 1.10, moderate burn severity = 2.25 and high burn severity = 3.75. Nevertheless, a maximum 0.55 value was settled to stay within the same range established by for Panagos et al. (2015) recently burned areas. $\boldsymbol{C_t}$ factor mean values can be observed in Table 3b.

Burn severity classes were classified following the classification of the USGS FIREMON program (USGS, 2004) and based on the ***dNBR*** values obtained by Gómez-Sánchez et al. (2017) for the same burned area (Supplementary Figure 3).

The post-fire management measures were mapped using geographic data provided by the local administration and aerial images taken in 2015 by the Spanish Geographic National Institute (IGN). The measures explained above, were introduced as modifications of the input layers of the post-management scenario. Channel measures were included to the index inputs by the DEMs. On the other hand, hillslope measures were included by modifying the post-management C-factor map. Log and contour felled log debris barriers were considered to increase the flow impedance of the terrain, depending the C-factor value, on their efficiency retaining sediment fluxes. This efficiency value was assigned to the hillslope barriers based in two studies. The first study was performed by Badía et al. (2015) in an area located in NE-Spain with similar conditions to ours. Among the post-fire treatments in this burned area, we can find that log barriers were built to control soil erosion, having these features an efficiency retaining sediments of 83%. On the other hand, contour felled log debris barriers, were assigned a lower efficiency, based on Aristeidis and Vasiliki (2015) study in Greece. This study was performed at a burned Aleppo pine forest under similar climatic conditions, and the efficiency of this measure was only of a 45%. These efficiencies were applied considering that the maximum value flow impedance (100%) was C-factor = 0.001. Afforestation also modified the C-factor map; this modification was based on the data provided by García-Matallana et al. (2022) which was carried out at the previously described afforested areas. After surveying afforested and control plots, they observed coverture differences between these control plots and the reforested ones of 30.51% (the mechanical subsoiling) and 19.79% (mechanical digging) (Supplementary figure 4). Based on these differences, the shrub coverture layer of those areas was modified for every SIOSE polygon where afforestation took place. Finally, the skid trails were also mapped, taking similar C-factor values to those of the other trails in the burned area.

In González-Romero et al. (2021), the catchment outlets were selected as computation target, with the aim of evaluating the medium- and long-term sediment connectivity processes where sediment accumulation and transport take place also in the channels (Murphy et al., 2019). In this study, the stream system of each catchment was selected as computation target, in order to obtain the spatial patterns and values of hillslope–channel SC that is the predominant process of sediment

delivery during short and intense episodes defined as those within which all eroded soils are transported out the sub-basins without deposition during a hydrological event (Gao and Puckett, 2012). To set the stream system as the target of the computation (AIC_{STR}), the flow-direction map was modified. Those pixels located in the stream system were given a value of zero, generating a mask to modify the flow direction map. This computation setup only affected the AIC downslope component (D_{dn}). We used a geomorphological criterion to draw the stream system mask, which means it was based on field observations despite using the upslope drainage area criteria. The latest approach has been used by other authors to establish the head of gully erosion in large areas (e.g. Gudino-Elizondo et al., 2018). However, this criterion does not consider landscape heterogeneities, in those areas where lithological and/or marked topographical changes appear. Therefore, our field-based criteria mirror the actual spatial pattern of concentrated overland flow and the beginning of incisive soil erosion features. Following the approach of López-Vicente et al. (2020).

2.6. AIC_{STR} values normalization

AIC_{STR} outputs depend on the computation target, the input values and their resolution, such as the catchment drainage area. To make the values of the different catchments comparable among them we normalized the outputs of Eq. (1) using equation (6) proposed by Lopez-Vicente et al. (2021):

$$AIC_{N-STR} = AIC_{STRi} \times \log_{10}(10 + FlowLength_{sim}) \quad (6)$$

where $\boldsymbol{AIC_{N\text{-}STR}}$ is the normalized index of SC.

The adjustment was applied to the outputs of each one of the catchments separately, using their own flow path length (m) and considering the target of the computation (stream network) as a reference. The modified flow direction map generated for the AIC_{STR} target was used to calculate the flow length map.

2.7. SSY field measurements

To evaluate the SC outputs with independent values from the computation, we measured the sediment stored behind the 10 new check-dams built in the five studied catchments (Fig. 2). This data was used to estimate the sediment yield (SY; $Mg{\cdot}ha^{-1}$) and area specific sediment yield (SSY; $Mg{\cdot}ha^{-1}{\cdot}year^{-1}$), which provide a measure of the erosion produced in the ten sub-catchments draining into the check-dams during a defined period. The topographic field surveys were carried out during the spring of 2019. To do so, we followed the sections method proposed by Díaz et al. (2014) and used a total station (LEICA TC405) and a high performance GNSS device (LEICA GPS1200). The chosen method has demonstrated high accuracy estimating the volume behind check-dams (Ramos-Diez et al., 2017). Additionally, six bulk density samples were taken at each sediment wedge using a manual drill and a 50-cm^3 cylinder. After that, samples were dry in an oven at 105 °C and weighted. Then, SY ($Mg{\cdot}yr^{-1}$) and SSY ($Mg{\cdot}ha^{-1}{\cdot}yr^{-1}$) were calculated as showed in Equations (7) and (8). Check-dams 3 and 5 were discarded from the analysis because of their small drainage area compared with the others, as drainage area has a significant influence over the estimation of SSY (Bellin et al., 2011).

$$SY = \frac{SV \cdot BD_{SED}}{TE} \times 100 \quad (7)$$

$$SSY = \frac{SY}{A} \quad (8)$$

where $\boldsymbol{SV}$ (m^3) is the accumulated sediment volume behind the check-dams; $\boldsymbol{BD}$ ($Mg{\cdot}m^{-3}$) is the sediments bulk density; $\boldsymbol{A}$ (ha) is the drainage area; and $\boldsymbol{TE}$ (%) is the sediment trap efficiency of the check-dams (Quiñonero-Rubio et al., 2016).

Check-dam location measured SSY and post-fire measures upstream the dam are shown in Table 4.

2.8. Statistical analysis

To make the statistical analysis, we divided the five catchments in a total of 929 sub-catchments, 677 in the burned area (Supplementary Figure 5); this division was performed based on the flow accumulation map (generated with the *Deterministic Infinity* algorithm). To evaluate the effects of barriers on $AIC_{N\text{-}STR}$ temporal changes, a one-way ANOVA analysis and a post-hoc Tukey test (95% of confidence) were performed. With this ANOVA, for the 677 burned sub-catchments, we compared treated and non-treated areas using the mean $AIC_{N\text{-}STR}$ values. Treated areas were categorized depending on their barrier density ($m{\cdot}ha^{-1}$) into two categories: Low density (<100 m ha^{-1}) and medium-high density (>100 m ha^{-1}). In afforested areas, a different procedure was followed due to the reduced zone they occupy. Instead of the sub-catchment analysis, $AIC_{N\text{-}STR}$ values were obtained for a total of 1200 random points distributed along the afforested areas (subsoiled and dug) and equivalent control areas of the same catchment. The different treatments were also compared using a one-way ANOVA and a post-hoc Tukey test.

To test the influence of the main sub-catchment characteristics and studied factors on $AIC_{N\text{-}STR}$ values, a Pearson correlation analysis was performed using the data of the 677 sub-catchments of the burned area. The studied factors were the sub-catchment area, slope (mean, maximum and minimum), roughness of the terrain (mean), stream density, C factor (mean), severity (mean dNBR value) and permeability (mean).

Linear regression models were fitted to explain the relationship between the changes on $AIC_{N\text{-}STR}$ between scenarios and the measured post-fire SSY. All the analysis were performed with the R Statistical Software v2.15.3.

3. Results

3.1. Hillslope-channel sediment connectivity

Attending the obtained $AIC_{N\text{-}STR}$ values, the functional ($AIC_{N\text{-}STR}F$) and structural ($AIC_{N\text{-}STR}S$) approaches showed significantly different outcomes for the two temporal scenarios: year 2012 ('12′ label) and year 2014 ('14′ label). Considering all the study area (Fig. 3), $AIC_{N\text{-}STR}S12$ showed higher SC values, ranging between −20.9 and −3.23, than those SC values obtained in $AIC_{N\text{-}STR}14$ (between −21.1 and −3.69). Conversely, the functional approach in the Pre-man scenario ($AIC_{N\text{-}STR}F12$) had the lowest values, ranging from −22.4 to −3.87. Independently of the approach or temporal scenario, the higher SC values were in the streams and in the closer areas to the channels and stepper slopes. The histogram of the different scenarios and approaches (Fig. 3) showed a normal distribution of the $AIC_{N\text{-}STR}$ data.

The structural-functional differences were also noticeable when considering the mean values of the burned area of each catchment (Table 5). Regarding $AIC_{N\text{-}STR}$ evolution –calculated as the difference between the two temporal scenarios ($\Delta AIC_{N\text{-}STR}F$)–, the functional approach increased $AIC_{N\text{-}STR}$ between 4.66% at Piñero and 5.84% at Grillo. However, and evaluating the changes in the structural approach ($\Delta AIC_{N\text{-}STR}S$), the $AIC_{N\text{-}STR}$ values suffered a mean decrease between a −2.73% at Grillo and a −4.60% at Piñero. Comparing between the different catchments burned area, the mean $AIC_{N\text{-}STR}$ values also showed differences. Piñero registered the highest connectivity in the different scenarios and dynamic conditions, namely: $AIC_{N\text{-}STR}$ F12 ($\bar{x}$ =-11.63), $AIC_{N\text{-}STR}S12$ ($\bar{x}$ =-10.60) and $AIC_{N\text{-}STR}F\&S14$ ($\bar{x}$ =-11.09). Grillo was the catchment with the lowest values of sediment connectivity in the three computations: with $AIC_{N\text{-}STR}F12$ ($\bar{x}$ =-12.73), $AIC_{N\text{-}STR}S12$ ($\bar{x}$ =-11.67) and $AIC_{N\text{-}STR}F\&S14$ ($\bar{x}$ =-11.99). The rest of the catchments took intermediate values between those as it can be observed in Table 5.

Table 4
Main characteristics of the check-dams and upstream measures in the five catchments. Afforestation; Hillslope barriers; Rock check-dams; Bulk density; TE: sediment trap efficiency; SSY: area specific sediment yield.

Catchment	Check-dam	UTM X	UTM Y	Area (ha)	Rock check-dams upstream (contributed area)	Hillslope barriers upstream	Afforestation area upstream	Volume	Bulk density	TE	SSY
					(nº; ha)	($m \cdot ha^{-1}$)	(%)	(m^3)	($Mg \cdot m^{-3}$)	(%)	($Mg \cdot ha^{-1} \cdot y^{-1}$)
Postes	**1**	610269	4252670	143	6 (18.57)	32.12	–	304.53	1.018	30.9	1.20
Conejo	**2**	611678	4251797	194	–	119.28	–	585.70	1.002	38.8	1.31
Grillo	**3**	614441	4251178	9	–	–	–	160.47	1.178	78.9	4.76
Grillo	**4**	614291	4250785	87	6 (13.22)	61.58	–	209.53	1.172	33.7	1.48
Piñero	**5**	613360	4249533	3	–	11.49	24	45.02	1.034	75.9	3.45
Piñero	**6**	613389	4249534	34	1 (8.31)	19.68	10	163.58	1.027	50.3	1.64
Piñero	**7**	613847	4249857	65	16 (31.2)	–	–	135.45	0.982	30.4	1.17
Piñero	**8**	612545	4249847	47	–	–	–	115.58	1.259	34.1	1.63
Rayares	**9**	609399	4249982	66	4 (7.63)	–	–	389.52	1.047	55.3	1.96
Rayares	**10**	608724	4250783	51	8 (8.91)	–	–	71.32	0.747	22.7	0.81

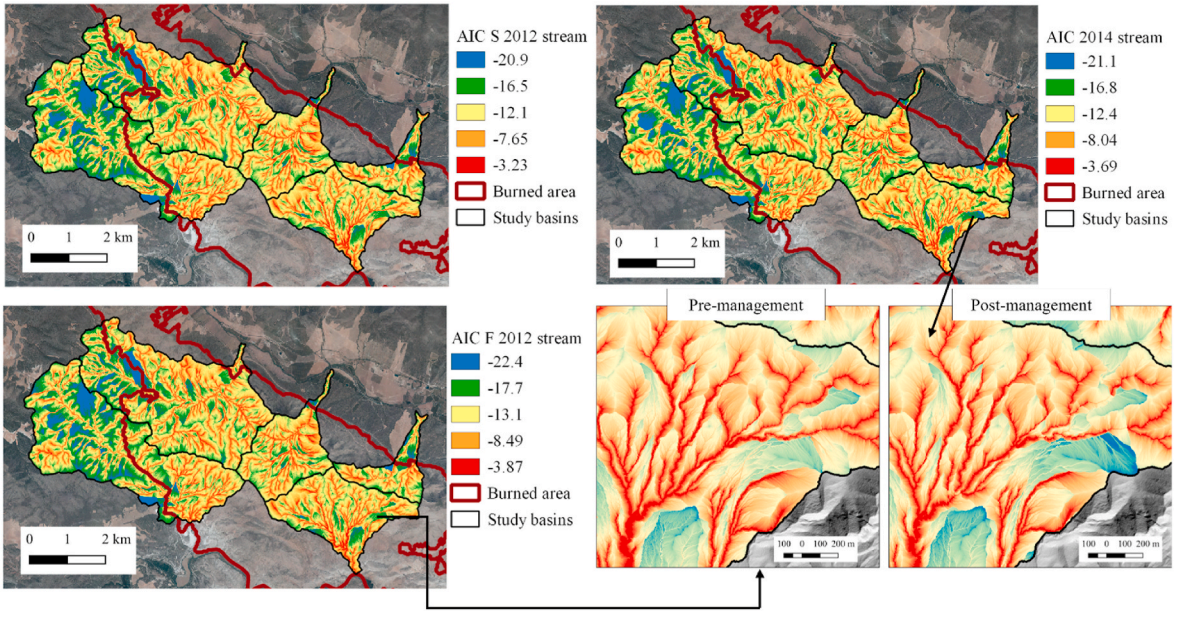

Fig. 3. Maps of $AIC_{N\text{-}STR}$ of the pre-management scenario for the structural (top left map), the functional (bottom left map) andthe post-management scenario (top right map). Additionally, zoom maps for the two scenarios are shown in the bottom right.

Table 5
Mean values of $AIC_{N\text{-}STR}$ and temporal changes ($\Delta AIC_{N\text{-}STR}$; %) per catchment and approach (only the burned area was considered) in the estimated structural ('S') and functional ('F') sediment connectivity.

Catchment	Pre-management		Post-management	Temporal changes	
	$AIC_{N\text{-}STR}F12$	$AIC_{N\text{-}STR}S12$	$AIC_{N\text{-}STR}F\&S14$	$\Delta AIC_{N\text{-}STR}F$	$\Delta AIC_{N\text{-}STR}S$
Conejo	−11.86	−10.81	−11.27	4.98%	−4.21%
Grillo	−12.73	−11.67	−11.99	5.84%	−2.73%
Piñero	−11.63	−10.60	−11.09	4.66%	−4.60%
Postes	−12.41	−11.37	−11.77	5.16%	−3.50%
Rayares	−12.11	−11.08	−11.47	5.29%	−3.45%

3.2. Sediment connectivity at sub-catchment scale

Correlations between sub-catchment characteristics and $AIC_{N\text{-}STR}$ are shown in Table 6. The factors which had a higher correlation with $AIC_{N\text{-}STR}$ were the main physiographic characteristics (slope variables and roughness of the terrain) and stream density for the two temporal scenarios. $AIC_{N\text{-}STR}$ values had a higher correlation with stream density ($r_{12} = 0.62$; $r_{14} = 0.64$) in comparison with slope variables, namely, with the mean slope ($r_{12} = 0.33$; $r_{14} = 0.44$) and maximum slope ($r_{12} = 0.35$; $r_{14} = 0.46$). Variables like roughness of the terrain ($r_{12} = 0.21$; $r_{14} = 0.23$) and soil permeability ($r_{12} = 0.16$; $r_{14} = 0.16$) had also significant correlations with $AIC_{N\text{-}STR}$. Slope variables were closely related between them even though mean slope values were more closely related to maximum values ($r_{12} = 0.70$; $r_{14} = 0.67$) than minimum values ($r_{12} = 0.39$; $r_{14} = 0.38$) at the two temporal scenarios; this minimum slope factor did not show a significant correlation with the mean values of $AIC_{N\text{-}STR}$. Vegetation coverage variables as Fire Severity or C-RUSLE were correlated between them ($r_{12} = 0.20$; $r_{14} = 0.15$) and soil permeability, and also showed significant correlations with $AIC_{N\text{-}STR}$, but with very low *r* values ($r_{12} = 0.10$; $r_{14} = 0.11$). The $AIC_{N\text{-}STR}$ values were not correlated with the sub-catchment area ($r_{12} = 0.06$; $r_{14} = 0.07$), but the area was significantly related with slope variables.

3.3. Hillslope measures performance

Hillslope barriers were effective reducing $AIC_{N\text{-}STR}$, since meaningful differences on $\Delta AIC_{N\text{-}STR}$ were observed depending on the density of hillslope barriers for the two approaches (functional and structural) (Fig. 4). When considering the functional approach –that includes the

Table 6
Pearson correlation matrix relating AIC with the sub-catchments' main characteristics: area (mean area); mean slope at the pre-man and the post-man scenarios (Mean slp 12; Mean slp 14); maximum slope at the pre-man and the post-man scenarios (max slp12; max slp14); minimum slope at the pre-man and the post-man scenarios value (min slp12, min slp14); mean roughness of the terrain (RT); stream density (Str Density), mean C factor at the pre-man and the post-man scenarios (C 12; C 14), mean soil permeability value (Kp); Mean $AIC_{N\text{-}STR}$ value at the pre-man and the post-man scenarios ($AIC_{N\text{-}STR}$ 12; $AIC_{N\text{-}STR}$ 14) Significant correlations (*p < 0.05; **p < 0.01, ***p < 0.001).

	area	Mean slp 12	max slp12	min slp12	RT	Str Density	Severity	C 12	Kp	$AIC_{N\text{-}STR}$ 12
	(ha)	(%)	(%)	(%)	–	($m{\cdot}ha^{-1}$)	–	–	–	–
area	1									
Mean slp 12	0.32***	**1**								
max slp 12	0.33***	0.70***	**1**							
min slp 12	−0.10*	0.39***	0.17*	**1**						
RT	−0.001	−0.26**	−0.21**	−0.15*	**1**					
Str Density	−0.09	0.01	0.18**	0.001	−0.072	**1**				
Severity	0.02	0.06	0.08	0.03	0.0038	0.07	**1**			
C 12	−0.07	0.03	0.04	0.05	0.017	0.05	0.20**	**1**		
Kp	−0.08	−0.065	−0.061	−0.014	0.12*	0.086	0.11*	0.091	**1**	
$AIC_{N\text{-}STR}$ 12	0.06	0.33**	0.44***	−0.06	−0.21**	0.62***	0.08	0.1*	0.16*	**1**
	area	**Mean slp 14**	**max slp14**	**min slp14**	**RT**	**Str Density**	**Severity**	**C 14**	**Kp**	**$AIC_{N\text{-}STR}$ 14**
	(ha)	**(%)**	**(%)**	**(%)**	**-**	**($m{\cdot}ha^{-1}$)**	**-**	**-**	**-**	**-**
area	**1**									
Mean slp 14	0.32***	**1**								
max slp 14	0.31***	0.67***	**1**							
min slp 14	−0.08	0.38***	0.14*	**1**						
RT	0.037	−0.23**	−0.21**	−0.081	**1**					
Str Density	−0.09	0.01	0.20**	−0.13*	−0.08	**1**				
Severity	0.02	0.06	0.06	0.08	0.05	0.07	**1**			
C 14	−0.10	0.01	−0.002	0.02	0.0051	0.04	0.15*	**1**		
Kp	−0.08	−0.06	−0.074	0.08	0.1*	0.085	0.11*	0.1*	**1**	
$AIC_{N\text{-}STR}$ 14	0.07	0.35***	0.46***	0.08	−0.23**	0.64**	0.10	0.11*	0.16*	**1**

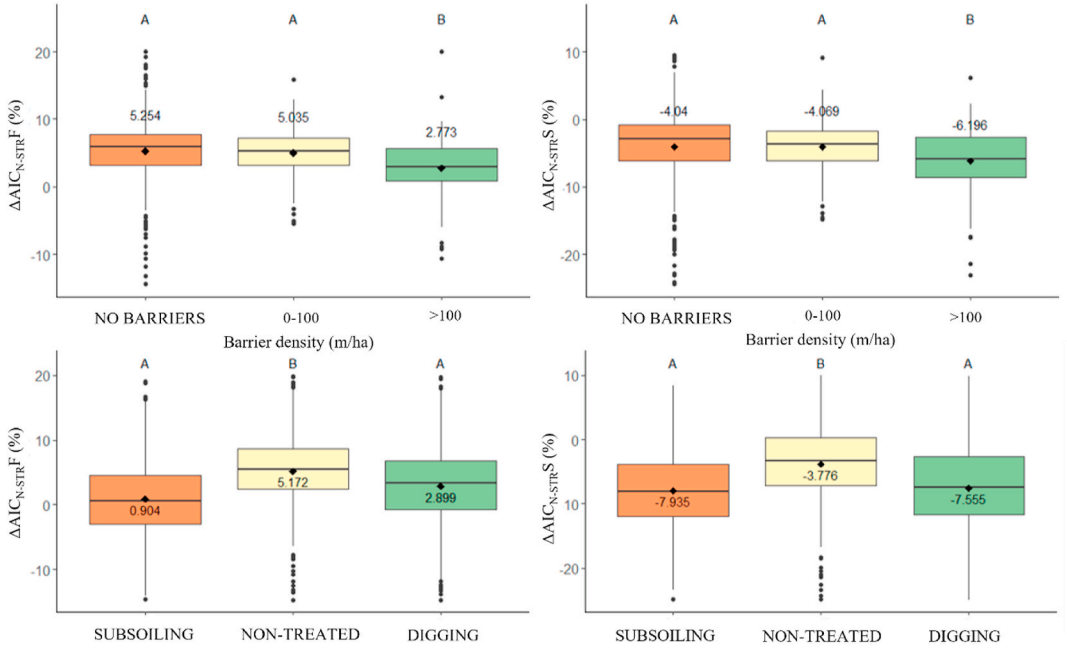

Fig. 4. Relationship between the temporal changes of estimated sediment connectivity ($\Delta AIC_{N\text{-}STR}$; %) and barriers density (m ha^{-1}; 0–100, >100 and no barriers) and afforestation treatment (Subsoiling, Digging and non-treated). Those boxplots with different capital letters had significant differences according to the post-hoc Tukey test results. Mean values are represented with a black diamond and numerically; Boxes represent the interquartile range; Median values are indicated by a line across the box; The "whiskers" finish at the maximum and minimum value and outliers are represented with black dots.

rainfall erosivity factor–, $AIC_{N\text{-}STR}F$ values increased between temporal scenarios regardless of the treatment. The highest mean increase was recorded at the sub-catchments without barriers with an increase of the 5.254%. The sub-catchments where the barriers were built with a low density (<100 m ha^{-1}) recorded similar values of $\Delta AIC_{N\text{-}STR}F$ than the non-treated ones with a mean value of 5.035%. Furthermore, the high-density hillslope barriers sub-catchments (>100 m ha^{-1}) had the lowest SC increment with a $\Delta AIC_{N\text{-}STR}F$ value of 2.773%. From a structural SC approach, the results were different and the $\Delta AIC_{N\text{-}STR}S$ values were negative corresponding with a SC decrease between temporal scenarios. At the sub-catchments without barriers, a decrease of structural connectivity was observed ($\Delta AIC_{N\text{-}STR}S = -4.04\%$). A similar mean value

was also observed at the low barrier density sub-catchments with $\Delta AIC_{N\text{-}STR}S = -4.069\%$. The greatest mean SC decrease was observed in the sub-catchments with a higher density of barriers, with $\Delta AIC_{N\text{-}STR}S = -6.196\%$. The ANOVA and Tukey tests results revealed that no significant differences were observed between those sub-catchments with a low density of hillslope barriers (<100 m ha^{-1}) and the ones without barriers for both structural and functional approaches. However, when the statistical analysis was focused on the sub-catchments with high barrier density (>100 m ha^{-1}), the differences were significant with lower $\Delta AIC_{N\text{-}STR}F$ and $\Delta AIC_{N\text{-}STR}S$.

Afforestation resulted in meaningful $AIC_{N\text{-}STR}$ changes between the two temporal scenarios. The two treatments (subsoiling and digging) resulted in lower $AIC_{N\text{-}STR}$ values with respect to the non-treated areas (Fig. 4). For the functional approach, non-treated areas had a mean $\Delta AIC_{N\text{-}STR}F$ of 5.172%. Reforested areas had lower $\Delta AIC_{N\text{-}STR}F$ values, the areas with the digging soil preparation had a $\Delta AIC_{N\text{-}STR}F$ value of 2.899%, whereas the subsoiled areas had even lower $AIC_{N\text{-}STR}$ increases ($\Delta AIC_{N\text{-}STR}F = 0.904\%$). The trend from the structural point of view was similar, and non-treated areas had the lowest $AIC_{N\text{-}STR}$ decrease ($\Delta AIC_{N\text{-}STR}S = -3.776\%$). Digging and subsoiling areas showed a greater decrease with a $\Delta AIC_{N\text{-}STR}S$ value of −7.555% and −7.935%, respectively. According to the ANOVA and Tukey HSD tests results, subsoiling and digging areas had significantly lower $\Delta AIC_{N\text{-}STR}F$ and $\Delta AIC_{N\text{-}STR}S$ than the changes obtained in the non-treated areas.

3.4. Channel measures performance

The effectiveness of channel disconnectivity measures of upstream areas was observed at the $AIC_{N\text{-}STR}$ maps (Fig. 5), which shows a clear disconnected area in Piñero (close to check-dam No. 7). In general, flux disconnectivity can be observed immediately upstream of the concrete check-dams (black square in the map) and in those channels where small rock check-dams (rock check-dams; crosses in the map) were built alienated. This reduction of $AIC_{N\text{-}STR}$ was observed in the surrounding slopes upstream the structures.

3.5. Sediment connectivity linked to the SSY

The relationship between the measured SSY and the $AIC_{N\text{-}STR}$ differences between the two temporal scenarios ($\Delta AIC_{N\text{-}STR}$) for the concrete check-dams' sub-catchments was positive (Fig. 6). The correlation coefficient (r) was 0.426 for $\Delta AIC_{N\text{-}STR}F$ and 0.508 for $\Delta AIC_{N\text{-}STR}S$. The sub-catchments No. 6, 8 and 9, where hillslope and channel measures

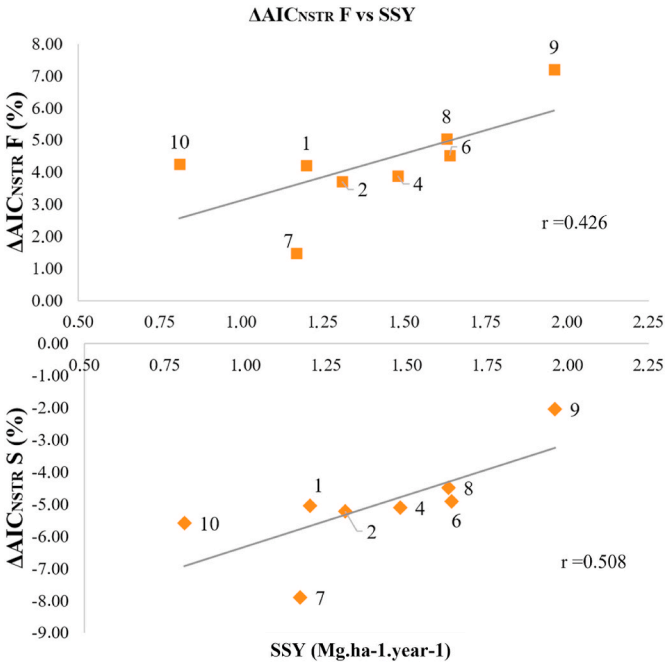

Fig. 6. Relationship between the temporal changes of estimated sediment connectivity ($\Delta AIC_{N\text{-}STR}$; %) at each check-dam sub-catchment and the measured values of area specific sediment yield (SSY; Mg·ha^{-1} yr^{-1}) in the check-dam.

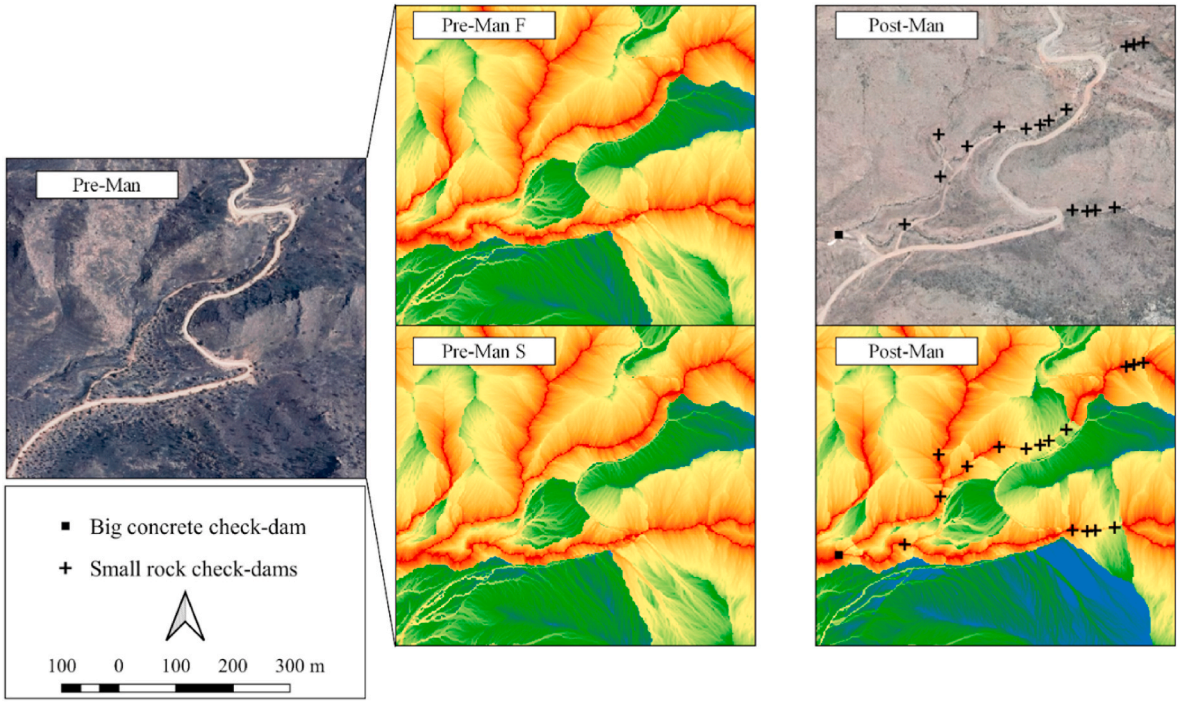

Fig. 5. Local effect of check-dams on $\Delta AIC_{N\text{-}STR}$ at the sub-catchment No. 7 for the pre-management (Pre-man) and post management (Post-man) scenarios and the functional (F) and structural (S).

were carried out with a lower density or were completely absent, recorded the higher SSY value. Conversely, sub-catchments No. 1, 2, 4, 7 and 10, which had a higher density of channel and hillslope measures, recorded lower SSY values. Those sub-catchments with a higher density of measures in the upstream part were also the ones where the lower $AIC_{N\text{-}STR}F$ increase and the higher $AIC_{N\text{-}STR}S$ increase between the temporal scenarios were recorded. The influence of the channel measures in $AIC_{N\text{-}STR}$ is clearly observed in the sub-catchment No. 7, which recorded mean $\Delta AIC_{N\text{-}STR}S$ and $\Delta AIC_{N\text{-}STR}F$ values that were considerably lower than those obtained in the other sub-catchments. This catchment was the one with the higher concentration of rock check-dams upstream the concrete check-dam.

4. Discussion

4.1. Catchment and sub-catchment response

As expected, higher AIC_N values were obtained than those reported in González-Romero et al. (2021), when targeting the outlet of the same study catchments and temporal scenarios instead of the channel network. These differences are explained because the downstream flow path is shorter when targeting the channel network, and thus, connectivity of the hillslopes increases drastically. This sediment transport dynamic is representative of the erosive processes derived from high intensity rainfall events, when the whole catchment is activated –in terms of soil erosion and sediment delivery (Grangeon et al., 2017)– and channel network effectively transports sediment out of the catchment, and thus, the connectivity within the slopes is multiplied. Intensive rain events in semi-arid areas can trigger flash flood with high peak flow that fit channel morphology by massive transport of sediments (Hooke, 2019). Attending to the differences between the mean values and changes of the five catchments, we can observe that Piñero and Conejo, had the highest values of SC for the two scenarios. This is explained by the fact that these catchments have the highest stream density, slope gradient and elongation ratio (more circular shape). Nevertheless, these two catchments also had a higher density of hillslope and channel measures which resulted in a higher reduction of structural $AIC_{N\text{-}STR}$ and a lower increase of functional $AIC_{N\text{-}STR}$ between scenarios.

The analysis at the sub-catchment scale reveals similar results. Among the studied factors, $AIC_{N\text{-}STR}$ values were significantly correlated with all the factors included in the index calculation, although those related with the slope gradient of the sub-catchments (especially the maximum slope values) had a higher influence on $AIC_{N\text{-}STR}$ values. These results contrast with those obtained by López-Vicente et al. (2020) who found that roughness of the terrain or land use factors showed the highest linear correlations with AIC_N values and underline other authors' field experiments like those performed by Badia and Marti (2008) or Nasta et al. (2017) who found that the hydrological response was clearly influenced by these factors. The low correlation of these factors in our study, and the more slope-driven SC changes may respond not only by the high influence of topography in the index output but also responds to the homogeneity of other factors, like the C-RUSLE which took very similar values in both scenarios. Permeability also had a significant but very low correlation with $AIC_{N\text{-}STR}$, in this respect, the permeability data used in this study was limited due to the lack of information. Furthermore, forest fires affect to soil physicochemical properties (Hedo et al., 2015), and those changes are not included in the AIC_N. Factors like soil water repellency are proved to change after fire affection and change soil permeability, and which have an accepted role in post-fire runoff generation and sediment transport (Stavi, 2019; Vieira et al., 2015). This factor though, is not easy to extrapolate from the hillslope/plot scale to the catchment scale due to its complexity, nonetheless, it seems interesting to study how to incorporate it to the aggregated weight factor of this index. The factor with the highest correlation with $AIC_{N\text{-}STR}$ that was observed in our study was stream density which directly respond with the way the index is calculated. The utilization of the stream mask to fix the channel network as the target of the computation, has an obvious and great influence on $AIC_{N\text{-}STR}$ results, which hinders the importance of develop fixed standards to establish the magnitude of the channel network in this type of studies. In our case, the followed field-based criterion supported by the flow accumulation data seems solid enough, but this factor should be taken into account when computing this index.

4.2. Post-fire measures effect on SC

The sub-catchments where hillslope measures were carried out, showed a significantly different behavior than untreated ones according to our computation results. The differences between treated areas (afforestation and hillslope barriers) and untreated ones are more marked when using $AIC_{N\text{-}STR}$ which is focused on lateral SC (hillslope-channel connectivity) and simulates net sediment transport through the channels. This underlines the importance of hillslope treatments to mitigate post-fire soil erosion at least under low intensity rainfall conditions (Robichaud et al., 2008).

Authors like Lopez-Vicente et al. (2021) who studied the effectiveness of hillslope barriers (with a mean density of barriers 340 m ha^{-1}) to reduce sediment connectivity in small catchments using high precision DEMs (0.05 × 0.05m) also obtained a reduction of AIC values attributable to hillslope barriers construction. Their study recorded a SC reduction between the Fire (pre-management) and Post-fire (post--management) scenarios of around 8.5% in the treated areas and a 5.2% in the untreated ones, attributing to hillslope barriers the 26.6% of the total decrease. The SC difference between untreated and high density treated areas in our study has similar magnitudes, with around a 2% SC reduction in areas with a density of barriers higher than 100 m ha^{-1}. They observed that the effectiveness of the barriers was not affected by the slope gradient obtaining a higher SC reduction for slopes higher than 60%. This higher effectiveness of hillslope barriers in very steep slopes cannot be properly assessed in our study area, since the construction of hillslope barriers was rarely performed in slopes gradients higher than 50–60% due to labor security and vegetal material unavailability at those areas, but authors like RobichaudRobichaud (2000) discouraged the installation of hillslope barriers in slopes greater than 40% and affirmed that gradients higher than 75% should be avoided.

In our index, when considering the higher rainfall erosivity of the post-man period, SC increased with respect the pre-man scenario (Functional approach) even in those areas with high density of hillslope barriers. This increase reveals that the structural disconnectivity ($\Delta AIC_{N\text{-}STR}S = -6.196\%$) created by vegetation recovery and hillslope barriers construction may disappear when considering more intense and erosive events ($\Delta AIC_{N\text{-}STR}F = +2.773\%$) even though treated areas respond better than untreated ones. These results are in accordance with the observed performance of hillslope barriers in the USA, where Robichaud et al. (2008) noted that these measures were only effective with short rainfall events that had a return period of 2 years and recommends that regional climatic conditions should be carefully considered before choosing this treatment. In this regard, having an index which is able to include these climatic conditions into the sediment connectivity computation, makes AIC recommendable to evaluate post-fire management measures. Nevertheless, further research must be done to clearly identify the threshold values of rainfall intensity and duration that drastically reduce the effectiveness of each treatment, so we can consider those events and include them in the R_t input.

Afforestation resulted in a higher reduction of $AIC_{N\text{-}STR}$ than hillslope barriers construction, by incrementing the coverage of the shrub layer independently of the applied soil preparation (subsoiling or digging), these measures can have a positive effect on seedling survival and performance by increasing water availability and rooting depth (Palacios et al., 2009). It is a well-known fact that an increase of vegetation coverage drastically reduces runoff generation and sediment transport from the hillslopes to the channel network, increasing interception and

roughness of the terrain (Sandercock and Hooke, 2011). Subsoiling areas had a higher coverture and performed better than digging ones, which may encourage to prioritize the use of this soil preparation technique, nevertheless, the higher impact caused in the soils by subsoiling due to the breaking of the petrocalcic horizon should be enough to discard it (Barberá et al., 2005). Furthermore, active afforestation techniques like plantation, are considered a measure which should only be considered when vegetation recovery is not expected and the activities which are associated to site preparation may increase the risk of soil erosion and loss (Vallejo and Alloza, 2012; Wittenberg et al., 2020). Our data is based on the field survey of García-Matallana et al. (2022) in the study area. The afforested area in this study case, was very small and by hence is not likely to be extrapolated to other sites with different climatic and ecological characteristics. Many studies report that site preparation techniques which implies high intensity soil disturbances are likely to produce enhanced soil erosion (Löf et al., 2012).

4.3. Sediment disconnectivity and sediment delivery linked to the SSY

The disconnectivity effect of the concrete check-dams and the rock check-dams lines on sediment and water flow can be clearly observed in Fig. 5. This effect is local, but a great $AIC_{N\text{-}STR}$ decrease upstream the dam and the continuity of the flow downstream it, can be representative of the functioning of check-dams during an intense rainfall event. That comes as a result of the introduction of the disconnectivity in the streams mask, which helps to overcome the deficiency of not being able to detect the check-dam structure in our DEM due to its coarse resolution (González-Romero et al., 2021). That observed disconnectivity produced by rock check-dams matches also with the $AIC_{N\text{-}STR}$ and SSY data observed on Fig. 5, where the sub-catchment of the concrete check-dam No. 7 experienced a meaningfully lower increase (functional approach) and a higher decrease (structural approach) of $AIC_{N\text{-}STR}$ between scenarios which responds to the presence of several rock check-dams built in the main channel which reduced the $AIC_{N\text{-}STR}$ value in that sub-catchment. The results of the other sub-catchments also have a good correspondence between $AIC_{N\text{-}STR}$ changes, observed SSY and post-fire intervention, with higher SSY and higher $AIC_{N\text{-}STR}$ increase (Functional approach) at sub-catchments 6, 8 and 9 which had less density of measures.

The observed correlation between $AIC_{N\text{-}STR}$ and the SSY rate measured for the catchment of the concrete check-dams was positive but was lower than the correlation between AIC_N values and SSY when targeting the outlet at the same sub-catchments and time scenarios (González-Romero et al., 2021). That underlines that the natural hydrological functioning of the study catchments during the studied periods is closer to the one simulated with a predominance of low intensity processes and sediment transport and deposition through the channels ($AIC_{N\text{-}OUT}$) rather than a torrential dynamic with effective sediment transport through the channel network ($AIC_{N\text{-}STR}$).

4.4. Post-fire management implication

Both post-fire management measures (channel and hillslope) have an influence in decreasing either lateral SC (hillslope measures) or longitudinal SC (channel measures) and this is reflected in the real sediment dynamics of the catchments. Disconnecting hillslopes via green treatments like hillslope barriers, afforestation or straw mulch application may be recommendable over the construction of "grey" infrastructures like check-dams (Lopez-Vicente et al., 2020). Nonetheless, the effectivity of these measures is conditioned by rainfall erosivity and under high intense events their effect may not be enough to stop extreme sediment transport processes.

Even though sediment connectivity indices have not been widely applied in post-fire management and their applicability to this topic can still be optimized, the use of the AIC_N index on burned areas can be already very useful for managers. This index is more sensitive than others to forest fires effects (Lopez-Vicente et al., 2020) and allows us to calculate in advance the effect on SC of carrying out different measures along the affected area. The observed differences between establish as target of the computation the channel network ($AIC_{N\text{-}STR}$) or the catchment outlet ($AIC_{N\text{-}OUT}$) as González-Romero et al. (2021) did, make each one of them more adequate to evaluate different effects and post-fire management measures. Both approaches provide useful information for the managers depending on the objective of the study. $AIC_{N\text{-}STR}$ as it is shown in this study is more useful to evaluate hillslope processes and thus to evaluate hillslope measures effectiveness, while $AIC_{N\text{-}OUT}$ its more suitable when we want to evaluate SC at a catchment scale or when we are trying to assess the risk of downstream infrastructures or habitats.

5. Conclusions

We can conclude that $AIC_{N\text{-}STR}$ reflected in a satisfactory way the effects of the different emergency stabilization measures. The correlation between sediment connectivity changes and the sediment yield of the monitored validation sub-catchments was positive, and the structural sediment connectivity reduction between scenarios also resulted in a decrease of the eroded sediment. The $AIC_{N\text{-}STR}$ index also reflected in a satisfactory way how intense rainfall events and high rainfall erosivity, can overcome the effect of post-fire management. Even though post-fire emergency stabilization measures proved to create a structural disconnectivity with respect to the pre-man scenario, when the more erosive rainfall conditions of the post-man scenario were considered, that effect was dissipated and $AIC_{N\text{-}STR}$ increased between scenarios. Furthermore, the possibility to fix different targets of the computation gives the AIC_N index great versatility and the possibility to be adapted to evaluate different situations depending on the objective and the requirements of the restoration.

These findings make the AIC_N index, an interesting and low input demanding tool for forest and land managers, not only to assess forest fire effects and plan the possible location of the treatments, but also to assess their effect in advance under different rainfall conditions. To optimize the application of AIC_N for post-fire management assessment, a better understanding of how the different factors that trigger runoff generation and soil erosion after fire affection can be included as inputs to the index and how post-fire stabilization measures interact with them under specific climatic conditions.

Data availability statement

The data that support the findings of this study are available from the corresponding author upon reasonable request.

Credit author statement

Javier González-Romero: Conceptualization, Methodology, Formal analysis, Writing – original draft. Manuel López-Vicente: Conceptualization, Methodology, Writing – review & editing. Elena Gómez-Sánchez: Resources. Esther Peña-Molina: Formal analysis. Pablo Galletero: Supervision. Pedro Plaza-Álvarez: Validation. Alvaro Fajardo: Validation. Jorge de las Heras: Supervision, Funding acquisition, Project administration: Daniel Moya: Supervision. Manuel Lucas-Borja: Conceptualization, Methodology, Writing- Reviewing and Editing,

Declaration of competing interest

The authors declare that they have no known competing financial interests or personal relationships that could have appeared to influence the work reported in this paper.

Acknowledgements

The authors thank the Regional Government of Castilla-La Mancha (Junta de Comunidades de Castilla-La Mancha) for supporting the study and providing information about the undertaken measures in the burned area. This study was supported by funds provided to the VIS4FIRE Spanish R&D project (RTA 2017-00042-C05-00) co-funded by the "Instituto Nacional de Investigación y Tecnología Agraria" (INIA) and FEDER programme. This study was done in the frame of the European Cooperation in Science and Technology (COST) action CA18135 'FIRElinks' (Fire in the Earth System: Science & Society). J. González-Romero holds a postdoctoral contract supported by the European Social Fund (ESF, EU). The authors declare no conflict of interest. E. Peña holds a scholarship (2020-PREUCLM-16032) from the UCLM and the European Social Fund (FSE). Pedro Antonio Plaza Álvarez holds a predoctoral fellowship from the Spanish Ministry of Education, Culture and Sport (FPU16/03296).

Appendix A. Supplementary data

Supplementary data to this article can be found online at https://doi.org/10.1016/j.jenvman.2022.115212.

References

Albert-Belda, E., Bermejo-fernández, A., Cerdà, A., Taguas, E.V., 2019. The use of Easy-Barriers to control soil and water losses in fi re-affected land in Quesada, Andalusia, Spain. Sci. Total Environ. 690, 480–491. https://doi.org/10.1016/j.scitotenv.2019.06.303.

Aristeidis, K., Vasiliki, K., 2015. Evaluation of the post-fire erosion and flood control works in the area of Cassandra (Chalkidiki, North Greece). J. For. Res. 26 (1), 209–217. https://doi.org/10.1007/s11676-014-0005-9.

Badia, D., Marti, C., 2008. Fire and rainfall energy effects on soil erosion and runoff generation in semi-arid forested lands. Arid Land Res. Manag. 22, 93–108. https://doi.org/10.1080/15324980801957721.

Badía, D., Sánchez, C., Aznar, J.M., Martí, C., 2015. Post-fire hillslope log debris dams for runoff and erosion mitigation in the semiarid Ebro Basin. Geoderma 237–238, 298–307. https://doi.org/10.1016/j. geoderma.2014.09.004.

Barberá, G.G., Martínez-Fernández, F., Alvarez-Rogel, J., Albadalejo, J., Castillo, V., 2005. Short- and intermediate-term effects of site and plant preparation techniques on reforestation of a Mediterranean semiarid ecosystem with Pinus halepensis Mill. N. For. 29 (2), 177–198. https://doi.org/10.1007/s11056-005-0248-6.

Bellin, N., Vanacker, V., van Wesemael, B., Solé-Benet, A., Bakker, M.M., 2011. Natural and anthropogenic controls on soil erosion in the internal betic Cordillera (southeast Spain). Catena 87, 190–200. https://doi.org/10.1016/j.catena.2011.05.022.

Boix-Fayos, C., Boerboom, L.G.J., Janssen, R., Martínez-Mena, M., Almagro, M., Pérez-Cutillas, P., Eekhout, J.P.C., Castillo, V., de Vente, J., 2020. Mountain ecosystem services affected by land use changes and hydrological control works in Mediterranean catchments. Ecosyst. Serv. 44, 101136. https://doi.org/10.1016/j.ecoser.2020.101136.

Borselli, L., Cassi, P., Torri, D., 2008. Prolegomena to sediment and flow connectivity in the landscape: a GIS and field numerical assessment. Catena 75 (3), 268–277. https://doi.org/10.1016/j.catena.2008. 07.006.

Burguet, M., Taguas, E.V., Gomez, J.A., 2017. Exploring calibration strategies of the SEDD model in two olive orchard catchments. Geomorphology 290, 17–28. https://doi.org/10.1016/j.geomorph. 2017.03.034.

Cavalli, M., Trevisani, S., Comiti, F., Marchi, L., 2013. Geomorphometric assessment of spatial sediment connectivity in small Alpine catchments. Geomorphology 188, 31–41. https://doi.org/10.1016/j. geomorph.2012.05.007.

Cavalli, M., Vericat, D., Pereira, P., 2019. Mapping water and sediment connectivity. Sci. Total Environ. 673, 763–767. https://doi.org/10.1016/j.scitotenv.2019.04.071.

Cerdà, A., Lucas-Borja, M.E., Úbeda, X., Martínez-Murillo, J.F., Keesstra, S., 2017. *Pinus halepensis* M. versus *Quercus ilex* subsp. *Rotundifolia* L. runoff and soil erosion at pedon scale under natural rainfall in Eastern Spain three decades after a forest fire. For. Ecol. Manag. 400, 447–456.

Chandrashekar, H., Lokesh, K.V., Sameena, M., Roopa, J., Ranganna, G., 2015. In: Dwarakish, G.S. (Ed.), Proc. Int. Conf. On Water Resources, Coastal and Ocean Engineering (Mangalore), vol. 4. Elsevier Procedia), pp. 1345–1353.

Díaz, V., Mongil, J., Navarro, J., 2014. Topographical surveying for improved assessment of sediment retention in check dams applied to a Mediterranean badlands restoration site (Central Spain). J. Soils Sediments 14, 2045–2056. https://doi.org/10.1007/s11368-014-0958-5.

Fernández-García, V., 2019. Effects of fire recurrence and burn severity in fire-prone pine ecosystems. PhD Thesis. In: Basis for Forest Management. Universidad de León, Spain.

Fernández, C., Fernández-Alonso, J.M., Vega, J.A., 2020. Exploring the effect of hydrological connectivity and soil burn severity on sediment yield after wildfire and mulching. Land Degrad. Dev. 31 (13), 1611–1621. https://doi.org/10.1002/ldr.3539.

Gao, P., Puckett, J., 2012. A new approach for linking event-based upland sediment sources to downstream suspended sediment transport. Earth Surf. Process. Landforms 37, 169–179. https://doi.org/10.1002/esp.2229.

García Matallana, R., Lucas-Borja, M.E., Gómez-Sánchez, M.E., Uddin, S.M.M., Zema, D. A., 2022. Post-fire restoration effectiveness using two soil preparation techniques and different shrubs species in pine forests of South-Eastern Spain. Ecol. Eng. 178, 106579. https://doi.org/10.1016/j.ecoleng.2022.106579.

Girona-García, A., Vieira, D., Silva, J., Fernández, C., Robichaud, P., Keizer, J., 2021. Effectiveness of post-fire soil erosion mitigation treatments: a systematic review and meta-analysis. Earth Sci. Rev. 217, 103611. https://doi.org/10.1016/j.earscirev.2021.103611.

Gómez-Sánchez, E., De las Heras, J., Lucas-Borja, M., Moya, D., 2017. Assessing fire severity in semi-arid environments: application in Donceles 2012 wildfire (SE Spain). Revista de Teledeteccion 49 (49), 103–113. https://doi.org/10.4995/raet.2017.7121.

González-Romero, J., López-Vicente, M., Gómez-Sánchez, E., Peña-Molina, E., Galletero, P., Plaza-Álvarez, P., Moya, D., De las Heras, J., Lucas-Borja, M.E., 2021. Post-fire management effects on sediment (dis)connectivity in Mediterranean forest ecosystems: channel and catchment response. Earth Surf. Process. Landforms 46 (13), 2710–2727. https://doi.org/10.1002/esp.5202.

Grangeon, T., Manière, L., Foucher, A., Vandromme, R., Cerdan, O., Evrard, O., Pene-Galland, I., Salvador-Blanes, S., 2017. Hydrosedimentary dynamics of a drained agricultural headwater catchment: a nested monitoring approach. Vadose Zone J. 16 (12) https://doi.org/10.2136/vzj2017.05.0113.

Gudino-Elizondo, N., Biggs, T.W., Castillo, C., Bingner, R.L., Langendoen, E.J., Taniguchi, K.T., Kretzschmar, T., Yuan, Y., Liden, D., 2018. Measuring ephemeral gully erosion rates and topographical thresholds in an urban watershed using unmanned aerial systems and structure from motion photogrammetric techniques. Land Degrad. Dev. 29, 1896–1905. https://doi.org/10.1002/ldr.2976.

Heckmann, T., Cavalli, M., Cerdan, O., Foerster, S., Javaux, M., Lode, E., et al., 2018. Indices of sediment connectivity: opportunities, challenges and limitations. Earth Sci. Rev. 187, 77–108. https://doi.org/10.1016/j.earscirev.2018.08.004.

Heckmann, T., Vericat, D., 2018. Computing spatially distributed sediment delivery ratios: inferring functional sediment connectivity from repeat high-resolution digital elevation models. Earth Surf. Process. Landforms 43 (7), 1547–1554. https://doi.org/10.1002/esp.4334.

Hedo, J., Lucas-Borja, M.E., Wic, C., Andrés-Abellán, M., De Las Heras, J., 2015. Soil microbiological properties and enzymatic activities of long-term post-fire recovery in dry and semiarid Aleppo pine (Pinus halepensis M.) forest stands. Solid Earth 6 (1), 243–252. https://doi.org/10.5194/se-6-243-2015.

Hooke, J.M., 2019. Extreme sediment fluxes in a dryland flash flood. Sci. Rep. 9, 1–12. https://doi.org/10.1038/s41598-019-38537-3.

Löf, M., Dey, D.C., Navarro, R.M., Jacobs, D.F., 2012. Mechanical site preparation for forest restoration. N. For. 43, 825–848. https://doi.org/10.1007/s11056-012-9332-x.

Lopez-Vicente, M., Ben-Salem, N., 2019. Computing structural and functional flow and sediment connectivity with a new aggregated index: a case study in a large Mediterranean catchment. Sci. Total Environ. 651, 179–191. https://doi.org/10.1016/j.scitotenv. 2018.09.170.

Lopez-Vicente, M., González-Romero, J., Lucas-Borja, M.E., 2020. Forest fire effects on sediment connectivity in headwater sub-catchments: evaluation of indices performance. Sci. Total Environ. 732, 139206. https://doi.org/10.1016/j.scitotenv.2020.139206.

Lopez-Vicente, M., Kramer, H., Keesstra, S., 2021. Effectiveness of soil erosion barriers to reduce sediment connectivity at small basin scale in a fire-affected forest. J. Environ. Manag. 278 (Pt 1), 111510. https://doi.org/10.1016/j.jenvman. 2020.111510.

Martínez-Murillo, J.F., Lopez-Vicente, M., 2018. Effect of salvage logging and check dams on simulated hydrological connectivity in a burned area. Land Degrad. Dev. 29 (3), 701–712. https://doi.org/10.1002/ldr.2735.

Martini, L., Faes, L., Picco, L., Irouméd, A., Lingua, E., Garbarino, M., Cavalli, M., 2020. Assessing the effect of fire severity on sediment connectivity in central Chile. Sci. Total Environ. 728, 139006. https://doi.org/10.1016/j.scitotenv.2020.139006.

Masselink, R.J.H., Keesstra, S.D., Temme, A.J.A.M., Seeger, M., Giménez, R., Casalí, J., 2016. Modelling discharge and sediment yield at catchment scale using connectivity components. Land Degrad. Dev. 27, 933–945. https://doi.org/10.1002/ldr.2512.

Murphy, B.P., Czuba, J.A., Belmont, P., 2019. Post-wildfire sediment cascades: a modeling framework linking debris flow generation and network-scale sediment routing. Earth Surf. Process. Landforms 44 (11), 2126–2140. https://doi.org/10.1002/esp.4635.

Nasta, P., Palladino, M., Ursino, N., Saracino, A., Sommella, A., Romano, N., 2017. Assessing long-term impact of land-use change on hydrological ecosystem functions in a Mediterranean upland agro-forestry catchment. Sci. Total Environ. 605–606, 1070–1082. https://doi.org/10.1016/j.scitotenv.2017.06.008.

Norman, J.B., 2015. Wildfire-Induced Flooding and Erosion Potential Modeling: Examples from Colorado, 2012 and 2013. In: 3rd Joint Federal Interagency Conference on Sedimentation and Hydrologic Modeling. https://doi.org/10.13140/RG.2.1.4422.1923. Reno, Nevada, USA.

Ortíz-Rodríguez, A.J., Muñoz-Robles, C., Borselli, L., 2019. Changes in connectivity and hydrological efficiency following wildland fires in Sierra Madre Oriental, Mexico. Sci. Total Environ. 655, 112–128. https://doi.org/10.1016/j.scitotenv. 2018.11.236.

Panagos, P., Borrelli, P., Meusburger, K., Alewell, C., Lugato, E., Montanarella, L., 2015. Land Use Policy Estimating the soil erosion cover-management factor at the European scale. Land Use Pol. 48, 38–50. https://doi.org/10.1016/j.landusepol.2015.05.021.

Palacios, G., Navarro-Cerrillo, R.M., del Campo, A., Toral, M., 2009. Site preparation, stock quality and planting date effect on early establishment of Holm oak (Quercus ilex L.) seedlings. Ecol. Eng. 35, 38–46. https://doi.org/10.1016/j.ecoleng.2008.09.006.

Quiñonero-Rubio, J.M., Nadeu, E., Boix-Fayos, C., de Vente, J., 2016. Evaluation of the effectiveness of forest restoration and check-dams to reduce catchment sediment yield. Land Degrad. Dev. 27, 1018–1031. https://doi.org/10.1002/ldr.2331.

Ramos-Diez, I., Navarro-Hevia, J., San Martín Fernández, R., Díaz-Gutiérrez, V., Mongil-Manso, J., 2017. Evaluating methods to quantify sediment volumes trapped behind check dams, Saldaña badlands (Spain). Int. J. Sediment Res. 32, 1–11. https://doi.org/10.1016/j.ijsrc.2016.06.005.

Rivas-Martínez, S., Díaz, T.E., Fernández-González, F., Izco, J., Loidi, J., Lousa, M., Penas, A., 2002. Vascular plant communities of Spain and Portugal. Addenda to the syntaxonomical checklist of 2001. Itinera Geobot. 15 (1–2), 5–922.

Robichaud Robichaud, P.R., 2000. Evaluating the Effectiveness of Postfire Rehabilitation Treatments. US Department of Agriculture, Forest Service, Rocky Mountain Research Station.

Robichaud, P.R., Wagenbrenner, J.W., Brown, R.E., Wohlgemuth, P.M., Beyers, J.L., 2008. Evaluating the effectiveness of contour-felled log erosion barriers as a post-fire runoff and erosion mitigation treatment in the western United States. Int. J. Wildland Fire 17 (2), 255. https://doi.org/10.1071/wf07032.

Robichaud, P.R., Wagenbrenner, J.W., Lewis, S.A., Ashmun, L.E., Brown, R.E., Wohlgemuth, P.M., 2013. Post-fire mulching for runoff and erosion mitigation. Part II: effectiveness in reducing runoff and sediment yields from small catchments. Catena 105, 93–111. https://doi.org/10.1016/j.catena.2012.11.016.

Rodrigo-Comino, J., López-Vicente, M., Kumar, V., Rodríguez-Seijo, A., Valkó, O., Rojas, C., Pourghasemi, H.R., Salvati, L., Bakr, N., Vaudour, E., Brevik, E.C., Radziemska, M., Pulido, M., Di Prima, S., Dondini, M., de Vries, W., Santos, E.S., Mendonça-Santos, M. de L., Yu, Y., Panagos, P., 2020. Soil science challenges in a new era: a transdisciplinary overview of relevant topics. Air. Soil Water Resour. 13 https://doi.org/10.1177/1178622120977491, 117862212097749.

Rulli, M.C., Offeddu, L., Santini, M., 2013. Modeling post-fire water erosion mitigation strategies. Hydrol. Earth Syst. Sci. 17 (6), 2323–2337. https://doi.org/10.5194/hess-17-2323-2013.

Sandercock, P.J., Hooke, J.M., 2011. Vegetation effects on sediment connectivity and processes in an ephemeral channel in SE Spain. J. Arid Environ. 75 (3), 239–254. https://doi.org/10.1016/j.jaridenv.2010.10.005.

Shakesby, R.A., 2011. Post-wildfire soil erosion in the Mediterranean: review and future research directions. Earth Sci. Rev. 105 (3–4), 71–100. https://doi.org/10.1016/j.earscirev.2011.01.001.

Stavi, I., 2019. Wildfires in grasslands and shrublands: a review of impacts on vegetation, soil, hydrology, and geomorphology. Water 11, 5. https://doi.org/10.3390/w11051042.

Vallejo, V., Alloza, J., 2012. Post-fire management in the Mediterranean basin. Israel J. Ecol. Evol. 58 (2), 251–264. https://doi.org/10.1560/IJEE.58.2-3.251.

Vieira, D.C.S., Malvar, M.C., Fernández, C., Serpa, D., Keizer, J.J., 2016. Geomorphology annual runoff and erosion in a recently burn Mediterranean forest – the effects of plowing and time-since-fire. Geomorphology 270, 172–183. https://doi.org/10.1016/j.geomorph. 2016.06.042.

Vieira, D.C.S., Fernández, C., Vega, J.A., Keizer, J.J., 2015. Does soil burn severity affect the post-fire runoff and interrill erosion response? A review based on meta-analysis of field rainfall simulation data. J. Hydrol. 523, 452–464. https://doi.org/10.1016/j.jhydrol.2015.01.071.

Wittenberg, L., van der Wal, H., Keesstra, S., Tessler, N., 2020. Post-fire Management Treatment Effects on Soil Properties and Burned Area Restoration in a Wildland-Urban Interface, Haifa Fire Case Study. Science of the Total Environment, p. 716. https://doi.org/10.1016/j.scitotenv.2019.135190. Article 135190.

Wohl, E., Brierley, G., Cadol, D., Coulthard, T.J., Covino, T., Fryirs, K.A., Grant, G., Hilton, R.G., Lane, S.N., Magilligan, F.J., Meitzen, K.M., Passalacqua, P., Poeppl, R. E., Rathburn, S.L., Sklar, L.S., 2019. Connectivity as an emergent property of geomorphic systems. Earth Surf. Process. Landforms 44, 4–26.